Tu C3 12

Laterally Constrained Surface Wave Inversion

T. Bardainne* (CGG), K. Garceran (CGG), M. Retailleau (CGG), X. Duwattez (CGG), R. Sternfels (CGG), D. Le Meur (CGG)

Summary

We propose a laterally constrained surface wave inversion to obtain a reliable near-surface shear-wave velocity field from Rayleigh wave measurements. This workflow is targeted at dense 3D broadband wide-azimuth land surveys, aiming to obtain reliable and realistic lateral shear-wave velocity variations pertinent with regard to surface or sub-surface information. We applied our methodology to a dataset acquired by Petroleum Development of Oman in the Sultanate of Oman. The S-wave velocity model obtained can be easily correlated to surface data, satellite map and time-reflectivity volume, hence demonstrating the potential of our method to build reliable and geologically consistent near-surface velocity models.

Introduction

Rayleigh wave modelling has become a common way of building a near-surface velocity model. Two different strategies are currently available: a non-linear stochastic inversion using a 1D forward modeller or a 3D elastic full-waveform inversion. As we wish to process and invert surface waves from a dense broadband Wide-Azimuth (WAZ) survey, 3D elastic full waveform modelling appears to be too expensive when considering the expected bandwidth (from 1 to 15 Hz), the area extension (hundreds of sq. km) and the number of shots and receivers(~ 6 billion traces). Hence, we focus on a method using a fast 1D forward modelling engine. We implement a laterally constrained surface wave inversion procedure in order to obtain a geologically consistent and reliable near-surface shear-wave velocity field from Rayleigh waves. This workflow is applied to a dense 3D WAZ land survey acquired by Petroleum Development of Oman (PDO) in the Sultanate of Oman.

Background

Amongst others, Duret et al. (2016) propose a three-step workflow to process and invert Rayleigh waves. The first step consists in an accurate frequency-dependent travel-time measurement for each selected source-receiver pair, in which the phase difference between two adjacent traces is used to derive the phase velocity. Then, a frequency-dependent surface-wave velocity tomography is performed using the picked travel-times. Finally, the frequency-dependent phase velocity volume obtained with the tomography is inverted to deliver an S-wave near-surface velocity model. However, the estimation of a geologically meaningful shear-wave velocity volume remains challenging on land surveys, mainly due to rapid lateral variations of the near-surface structure. Due to the ill-posed nature of the surface wave inversion problem, it becomes difficult to distinguish real lateral variations from intrinsic inversion uncertainties. To address this issue, we consider that geological consistency such as horizon continuity should be incorporated as a constraint to the inversion scheme. In this work, we introduce a new algorithm in order to better resolve the lateral variations of the inverted S-wave velocity field. This new approach improves the last step of our workflow. It follows the tomographic inversion of phase and group velocities of Rayleigh wave, thus a regularized Rayleigh wave dispersion function $\boldsymbol{V_{\mathbf{Rayleigh}}}(< \mathbf{x}, \mathbf{y}, \mathbf{f} >)$ is taken as a starting point in the inversion.

Method

Our surface wave inversion algorithm is based on the combination of a stochastic inverse problem and a fast multi-mode Rayleigh phase and group velocity modeller (Shapiro et al., 1997). In order to enhance the parameter space exploration, we used a parallel simulated annealing inversion process (Ram et al., 1996). This algorithm provides an efficient exploration of complex parameter spaces characterized by numerous local minima, without the high cost specific to conventional simulated annealing. Our goal is to obtain a geologically consistent 3D shallow S-wave velocity model $\mathbf{Vs}(< \mathbf{x}, \mathbf{y}, \mathbf{z} >)$ by inverting the whole Rayleigh-wave dispersion volume instead of performing independent local inversions for each bin or receiver. The proposed global inversion scheme pictured in Figure 1 is the only way to introduce lateral constraints by interdependence of neighbourhood bins.

Firstly, a multi-grid iterative approach has been used in order to extract the regional information. At the first iteration, a global average dispersion law is calculated and inverted to provide a 1D regional trend of the S-wave velocity model. The survey is then split into sub-areas where the regional model previously obtained is used as an initial guess for the subsequent inversions of smaller scales. This operation is repeatedly performed until reaching the final bin size (Figure 1-a). This technique minimizes the dependence to the initial velocity model, as the regional information is taken as a starting point for an increasingly local inversion.

Secondly, we introduced the application of neighbourhood velocity perturbations into the parallel simulated annealing process. Indeed, the simulated annealing technique consists of a series of small perturbations to the velocity model and comparison of cost functions calculated with the 1D forward modelling using the new velocity model and the reference one. By introducing neighbourhood variations, we invert a small set of dispersion laws together, each characterized by its own S-wave velocity model, but all linked by a laterally consistent perturbation of the velocity model, according to

a Gaussian-scaled part of the central perturbation (Figure 1-b). The cost functions are then calculated independently and summed to provide a cost function averaged over the neighbourhood. This technique allows models to be inverted in a laterally consistent way, minimizing the non-uniqueness of the solution by constraining the range of possible models.

Thirdly, the last technique we employ is an additional regional cost function which measures the lateral inconsistency of the current velocity model. For a given model, we calculate the statistical dispersion of the S-wave velocity model in the horizontal spatial directions. This value is sensitive to geologically implausible velocity variations, thus better constraining the resulting model to address issues related to inversion uncertainties and non-uniqueness of solutions (Figure 1-c). Note that we also independently apply the same measurement of dispersion along the z direction and add it to the global cost function in order to avoid inconsistent depth behaviour.

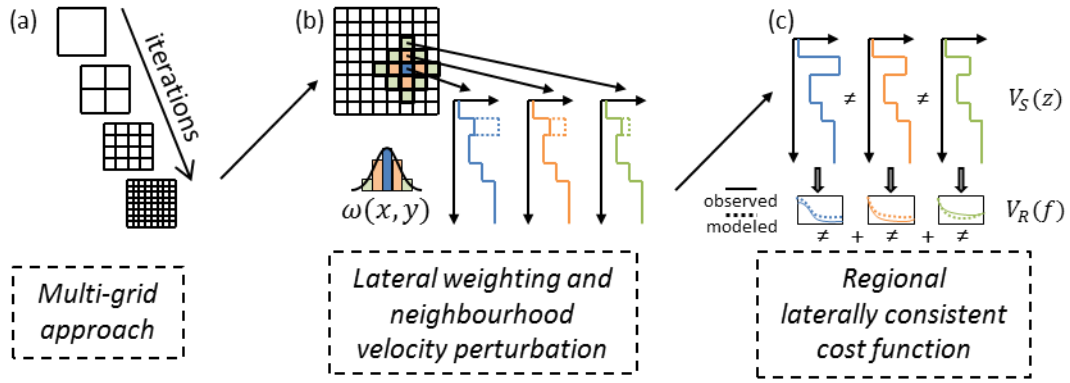

Figure 1: *Lateral constraint strategy: (a) a multi-grid iterative approach, (b) a neighbourhood velocity perturbation weighting applied during perturbation phase of simulated annealing, (c) a regional cost function obtained by summation of the regional velocity model lateral discontinuity cost function and every local modelled and observed dispersion curve misfit cost functions.*

Application on dataset

We test our methodology on a broadband 3D WAZ land survey acquired by PDO. The studied area (40 x 20 km) is characterized by 12.5 x 125 m spacing between receivers and 50 x 50 m spacing between sources. The three-step workflow using the new laterally constrained inversion is applied. An example of dispersion curves obtained along an inline during the first of the three steps is represented in Figure 2. The phase velocity of the Rayleigh-waves fundamental mode has been identified and automatically picked between 1.5 and 15 Hz based on a method described in Strobbia and Foti (2006).

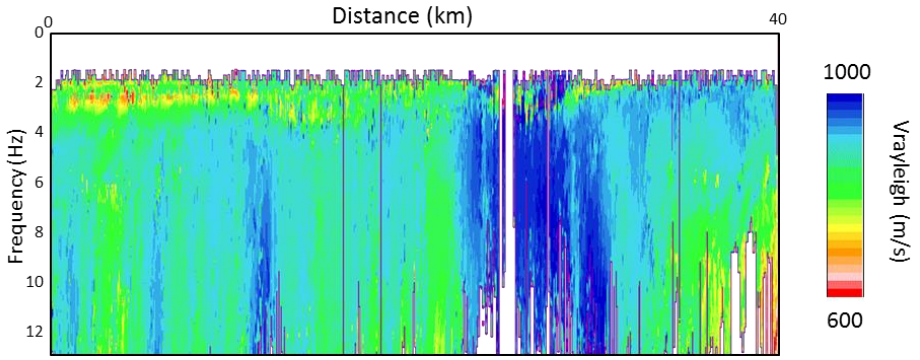

Figure 2: *Frequency-dependent Rayleigh wave phase velocity measurements. Dispersion curves are displayed along an inline. Velocities show important lateral variations and dispersive behaviour, which should be correlated to rapid lateral and depth variations of the near-surface Vs field.*

These frequency-dependent travel-time measurements delivered ~9 billion of picks. This dense but irregular dataset has been regularized using a multi-2d surface wave tomography as proposed by Lin and Ritzwoller (2011) (second step of our workflow).This regularized dispersion cube (100 x 100 m bin) has finally been inverted using the laterally constrained parallel simulated annealing scheme described above. The laterally constrained velocity model (Figure 3-b) is compared to an S-wave model obtained with a conventional inversion without lateral constraints (Figure 3-a). Comparison shows the contribution of the lateral constraints which introduce some geological and structural continuity that could not be obtained using a-posteriori smoothing of the conventional inversion. Some geological features which are not visible after the conventional inversion (due to the non-uniqueness of the solution) are now clearly highlighted.

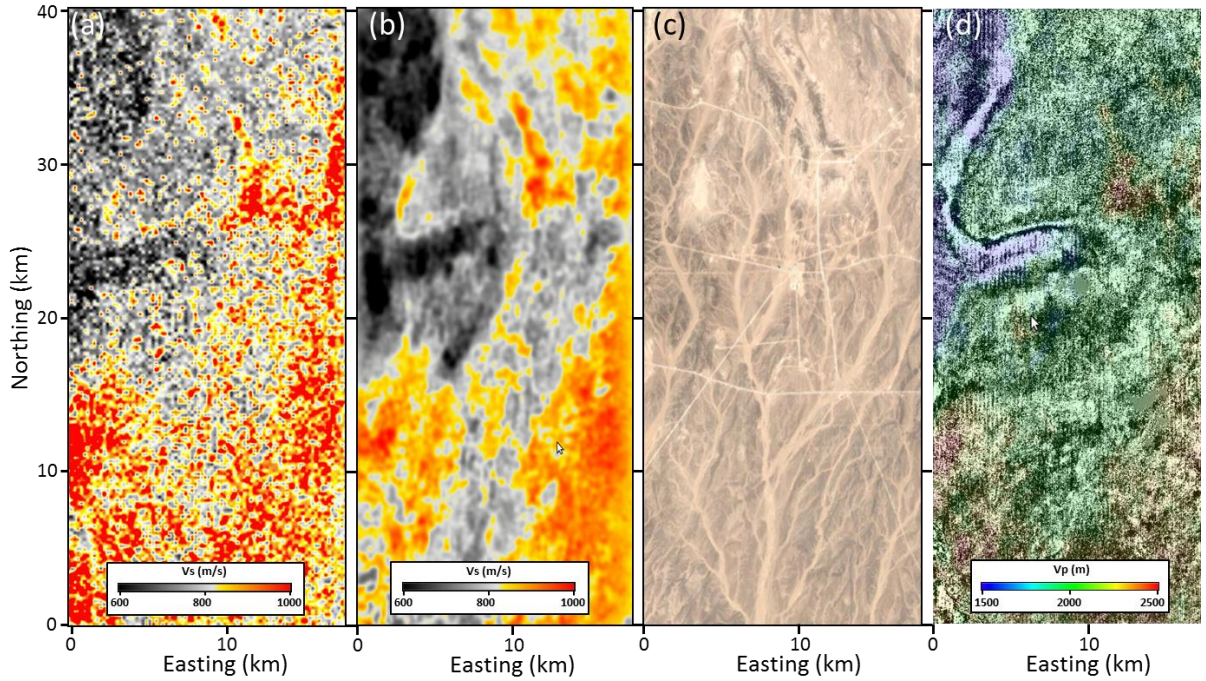

Figure 3*: Map view of S-wave velocity model obtained from surface wave inversion with surface and sub-surface external data: a) S-wave velocity model at 50m depth obtained with unconstrained inversion, b) S-wave velocity model at 50m depth obtained with laterally constrained inversion, c) satellite image, d) overlay of Vs(z) converted to Vp(t) (in colour) and the 100 ms time slice of the P-wave stack at (in grey).*

To check the consistency of our S-wave velocity model, we first compare a 50 m depth slice of the S-wave constrained velocity (Figure 3-b) to additional sub-surface attributes. A strong correlation of S-wave velocity is observed with the satellite image (Figure 3-c), revealing a complex near-surface under the gravel plain with small outcrops and dry wadi valleys. Furthermore, the change of soil coloration (top left hand side) is linked to a weaker S-wave velocity and can be explained by a lithological or facies change of the sub-surface. To confirm that the S-wave velocity correlates with the shallow sub-surface, we compare the latter with a time slice of the full stack at 100 ms (Figure 3-d). For this, we scale the S-wave velocity field to a pseudo P-wave velocity field using first a P to S regional conversion (using here a Vp/Vs 2.5 ratio) followed by a depth to time conversion. Knowing that we are in a desert with a deep water-table we consider that this hypothesis is reasonable in first approximation. The overlay between the pseudo P-wave field and the P-stack at 100 ms shows that the shape of main reflector visible on the P-stack section follows the lateral trend of the P-wave velocity field and confirms that the S-waves velocity model deduced from our surface wave inversion workflow allows to better define and to understand the shallowest part of the sub-surface.
In order to assess the vertical resolution of this pseudo P-wave velocity model, we compare it to a high resolution reflectivity volume obtained using surface-consistent predictive deconvolution operators (Retailleau, 2015). These operators show a more detailed image of the shallowest layers.

The superimposition of these two attributes, in time, shows that the lateral variations of inverted-converted P-wave velocity model strongly correlates in time with the shallow sub-surface reflectivity. Indeed, velocity contrasts follow the layers but also vertical lithological and facies changes (see arrows on Figure 4).

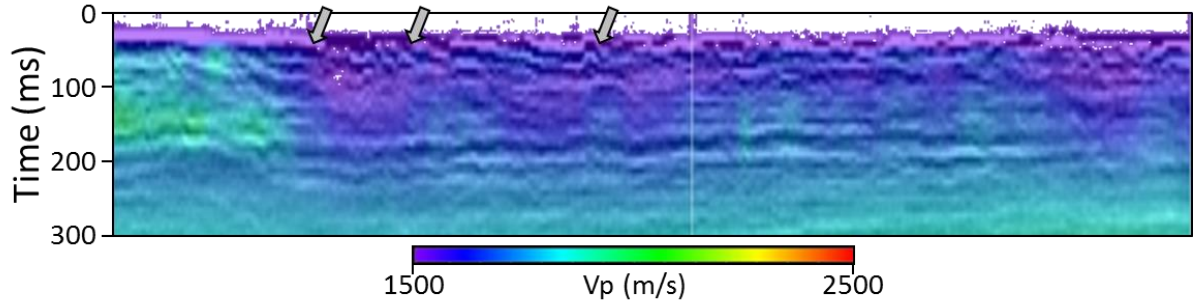

Figure 4: *Comparison of Vs(z) converted to Vp(t) with shallow sub-surface reflectivity obtained from the surface-consistent prediction deconvolution operators.*

Conclusion

This paper describes our latest improvements to better constrain our Rayleigh wave inversion workflow. The proposed scheme provides laterally and geologically consistent models which can be directly compared to surface or sub-surface attributes. The application of our methodology on a broadband 3D WAZ land survey shows that the estimated S-wave velocity is strongly linked to the surface and seismic data, the S-to-P and depth-to-time converted velocity model is correlated to time-reflectivity without taking into account the water influence for Vp in this dry near-surface. Results demonstrate the potential of our surface wave inversion workflow to build a geologically consistent near-surface S-wave velocity model. Conversion into a P-wave model using assumption or additional information can be used for subsequent processing steps such as elastic full-waveform inversion, depth imaging or shallow hazard studies.

Acknowledgements

We are grateful to Petroleum Development of Oman and the Ministry of Oil and Gas of the Sultanate of Oman for permission to present the data examples. We also thank CGG for permission to publish our results.

References

Duret F., Bertin F., Garceran K., Sternfels R., Bardainne T., Deladerriere N. and Le Meur D., [2016], Near-surface velocity modeling using a combined inversion of surface and refracted P-waves, The Leading Edge, 35(11):936-941.

Ram D.J., Sreenivas T.H., Subramaniam K.G., [1996], Journal of parallel and distributed computing 37 (2), 207-212

Retailleau M., Imaging the near surface using surface-consistent prediction operators: examples from the Middle-East, [2015], 77th EAGE Conference & Exhibition, Madrid.

Shapiro N.M., Campillo M., Paul A., Singh S.K., Jongmans D., and Sanchez-Sesma F.J.. [1997]. Surface-wave propagation across the Mexican Volcanic Belt and the origin of the long-period seismic-wave amplification in the Valley of Mexico, Geophys.J.Int. 128,151-166.

Strobbia C., and S. Foti, [2006], Multi-offset phase analysis of surface waves data (MOPA), Journal of Applied Geophysics, Volume 59, 300-313.